NUMERICAL ANALYSIS OF THE S-SHAPE CHARACTERISTIC IN A PUMP-TURBINE

G. Cavazzini – A. Covi - G. Pavesi – G. Ardizzon

Department of Industrial Engineering, University of Padova, Padova, Italy

ABSTRACT

The paper presents a numerical analysis of the unstable behaviour of a pump-turbine operating in turbine mode near the no-load condition. The entire machine, including the adduction and draft tube, was modelled and leakage flow rates were also considered in the numerical simulations.

To validate the numerical model, transient simulations were carried out by means of Ansys-CFX 14 on the pump-turbine model in stable operating conditions and the resulting performance was compared with the experimental ones.

Then, to study in-depth the unsteady phenomena which lead to the S-shape of the turbine characteristic, an unsteady numerical analysis, running through the flow-speed characteristic up to the pump-turbine brake zone during load rejection, was carried out. The flow rate was decreased at each time step, defined according to an impeller rotation of one degree, and about 20 impeller revolutions were necessary to completely define the unstable operating area.

NOMENCLATURE

B	width	[mm]	Q_m	mass flow rate	[kg s^{-1}]
C_m	meridional absolute velocity component	[ms^{-1}]	q_i,	flow rate of the channel i	[m^{3}s^{-1}]
c	blade mean line	[m]	n	shaft speed	[rpm]
D	diameter	[m]	n_b	number of blades	[-]
g	gravitational acceleration	[m s^{-2}]	$n_s=nQ^{0.5}/h^{0.75}$	specific speed	[m$^{0.75}$s$^{-1.5}$]
H	head	[m]	$Re=U_2D_2/\nu$	Reynolds number	[-]
K	mass flow rate reduction rate	[kg s^{-2}]	T	torque	[Nm]
k_{cm}	specific discharge factor	[-]	t	time	[s]
k_u	specific speed factor	[-]	U	peripheral velocity	[ms^{-1}]
P	mechanical power	[kW]	u,v,w	absolute velocity components	[ms^{-1}]
Q	flow rate	[m^{3}s^{-1}]			

Greek Symbols

α	absolute flow angle	[°]	ν	kinematic viscosity	[m^2/s]
β	relative flow angle	[°]	$\phi=C_{m2}/U_2$	flow coefficient	[-]
η	efficiency	[-]	ω	angular rotation speed	[s^{-1}]
λ	stagger angle	[°]	$\omega_s= \omega Q^{0.5}/h^{0.75}$	dimensionless specific speed	[-]
ρ	water density	[kg m^{-3}]			

Acronyms

BC	boundary condition	RMS	root mean square
GVO	guide vane opening	RPT	reversible pump-turbine
PS	pressure side	SS	suction side

Subscripts

1	runner outlet	bep	best operation point
2	runner inlet	ducts	inlet and outlet ducts
3	adjustable guide vanes outlet	GV	adjustable guide vanes
4	adjustable guide vanes inlet	r	runner

INTRODUCTION

The possibility of storing electric energy is a key issue when the production of electricity is based, for a substantial portion, on renewable sources. In fact, it is known that these sources are intermittent and not-programmable, so that they cannot meet the electricity user's demand.

Today, one of the most promising and tested way for storing electricity is the Pumped Hydro Storage Power Plant which is characterized by good dynamics (rapid changing from pumping mode to turbine mode) and provides high-quality energy.

The most common mechanical equipment adopted in the new generation of pumped-hydro energy storage is represented by Reversible Pump-Turbines (RPT), generally preferred to other technical arrangements due to their cost effectiveness.

Although Pumped Storage may solve several problems in the grid, fast and frequent changes between pumping and generating modes are required to pump-turbines, extending the operation of the machine at off-design conditions. However, the design of a pump-turbine is the result of compromise between contradicting targets, as pump and turbine performance, regulation capacity, efficiency and cavitation behaviour. The design criterion, much more focused on the behaviour in pumping mode, due to greater sensitivity of the decelerated flow field to boundary layer detachments and flow separations, may lead to the development of an unstable operating area (known as S-shaped region) that does not affect Francis turbines operating at the same conditions (Olimstad et al., 2012a).

In generating mode a RPT becomes unstable at low-load operating conditions close to runaway conditions and during load rejection (turbine brake). This unstable behaviour is reached during start-up and synchronization and is highly unwanted, since it increases start-up and switch-over times. Due to severe torque fluctuations caused by the instability development in this operating area, the RPT could be affected by sudden changes in working mode (from turbine to pump and vice versa) as well as by significant fluctuations of the head and flow rate with possible self-excited vibrations (Zhou et al., 2011; Gentner et al., 2012) or water hammers stressing not only the mechanical equipment but the whole power plant (Pejovic et al., 2011).

It has been observed that the appearance of these system instabilities and oscillations is closely linked to the negative slope of the head curve, determining a S-Shaped dimensionless speed discharge curve at constant guide vane opening (Olimstad et al., 2012b)
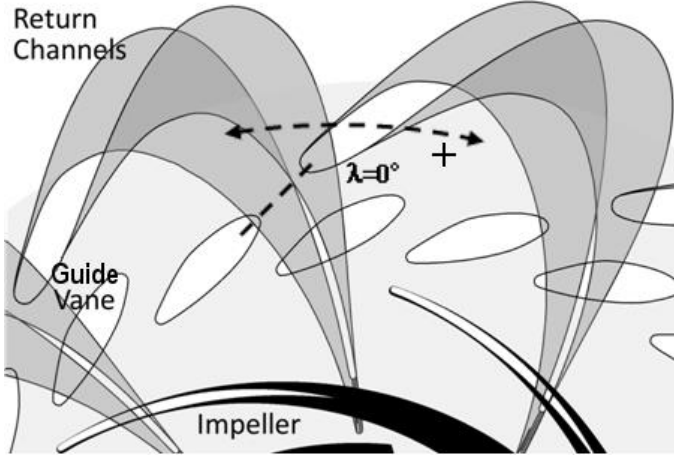
The causes of this S-Shaped characteristic seem to be related to the development of vortexes in the pump-turbine partially blocking the flow (Seidel et al., 2012; Wang et al., 2011; Sun et al., 2013). Some studies also have identified the development of stall cells rotating in the runner channels at 50-70% of the runner rotation frequency (Brennen, 1994; Hasmatuchi et al., 2011a; Hasmatuchi et al., 2011b; Widmer et al., 2011).

The aim of the paper is to study more in depth the onset and the characteristics of this unstable behaviour in order to understand the causes and effects of its development in RPT.

An in-depth analysis of the unsteady phenomena developing in a RPT operating in the S-shaped zone is presented. For a more complete comprehension of the phenomena, the RPT, including the leakage system, was modelled. The model was first validated in stable operating conditions by comparison with available experimental results. Then, the unstable behaviour of the reversible pump-turbine was investigated in-depth in order to characterize the unsteady phenomena developing during load rejection in the reversible pump-turbine and to identify the corresponding onset of vibrations both on runner blades and wicket gates.
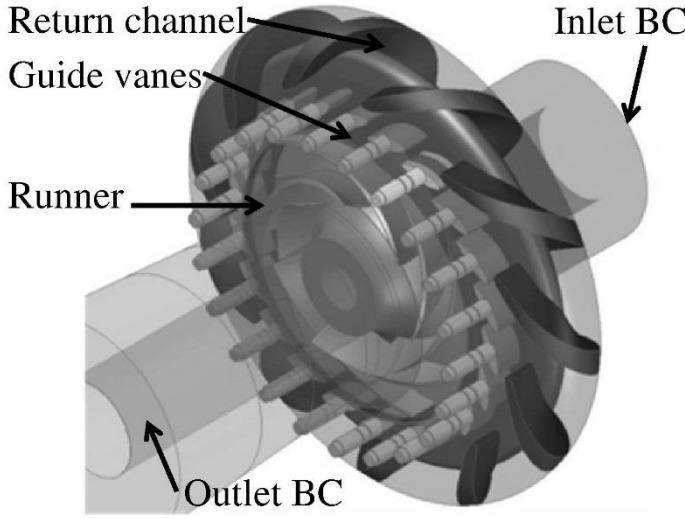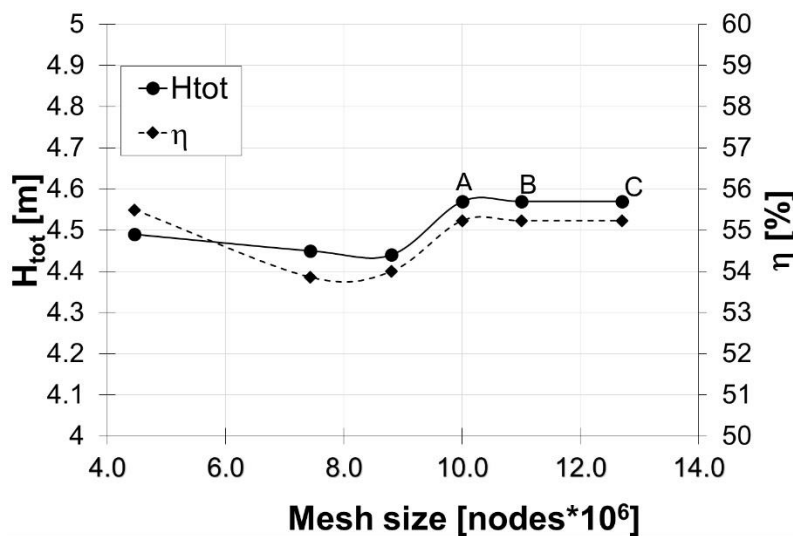
Fig. 1 Scheme of the tested configuration

Fig. 2 Guide vane reference azimuthal position (λ=0°)

Table 1 – Pump-turbine Data

Runner				
D_2 [mm]	B_2 [mm]	n_b	β_{2c} [°]	ϕ_{bep}
400	40	7	26.5	0.125
Guide Vanes				
D_3 [mm]	B_3 [mm]	n_b	α_{3c} [°]	λ [°]
410	40	22	10÷30	-8÷8
Return channel				
D_4 [mm]	B_4 [mm]	n_b	α_{4c} [°]	
516	40	11	30	

THE NUMERICAL MODEL

Numerical analyses were carried out by means of the commercial software ANSYS 14.0 on the first stage of a two stage reversible pump-turbine in turbine operating mode (fig. 1).

The scaled down model consists of a radial, shrouded impeller with 7 three-dimensional backward swept blades with a design specific speed n_s=37.6 $m^{0.75}s^{-1}$ (dimensionless design specific speed ω_s=0.71). Twenty-two adjustable guide vanes are coupled with 11 stay vanes. The guide vanes angles and their relative azimuthally position with the return channel vanes are continuously and independently adjustable. Tab. 1 reports the most important data of the considered pump-turbine.

In the analysed configuration, the radial gap between the trailing edge of the guide vanes and the runner tip was 10.5 mm, which is 5.25% of the impeller radius. The relative azimuthal position of the guide vanes was fixed rotating the system from the face to face configuration (λ=0°) to the configuration with the azimuthal position of the guide vanes 8° out of alignment (fig. 2). The guide vane opening (GVO) is equal to 18°.

The numerical model of the entire machine included inlet duct, return channel, guide vanes (distributor), runner, draft tube and leakage system.

The draft tube was discretized by a structured mesh of about 339500 elements with a y+ value not greater than 30 for the elements closest to the wall. As regards the runner, an O grid was performed. The stage head H and the stage efficiency were evaluated in preliminary tests to assure grid independent solution for the runner and to guarantee the capacity of numerical solution to

Fig. 3 Grid sensitivity analysis

3

capture the local pressure pulsations as well. Even if the sensitivity analysis highlighted a grid independent solution with about 200000 elements per passage (Fig. 3, mesh A), the intensity and the extent of the local pressure pulsations appear to be correctly evaluated only with grid greater than 300000 elements per passage (Fig. 3, mesh B). To be sure of the capacity of the numerical solution to capture local pressure pulsations in the whole domain, as a precautionary measure, the adopted number of elements was further increased (Fig. 3, mesh C).

The resulting runner computational domain used had a total of 3.7 million of cells with y+ values below 30. O-type grids were adopted for both the diffuser and the return channel discretization with about 3.55 and 5.11 million of cells, respectively. The leakage from the labyrinth seal was also considered and several H-blocks were built to describe the cavities.

The choice of the turbulence model is a key issue in CFD. According to the large flow separations expected in the unstable operating range, a Detached Eddy Simulation (DES) model was adopted. The shear stress transport k-omega model covered the boundary layer while the Smagorinsky-Lilly model was applied in detached regions. On both blades and wall surfaces, the boundary layer was assumed to be fully turbulent. All the interfaces between stator-rotor blocks were standard transient sliding interfaces and between stator-stator parts general connection interfaces were fixed.

At the inlet Boundary Condition (BC) the mass flow with stochastic fluctuations of the velocities with 5% free stream turbulent intensity was imposed with the value taken from the operating point experimentally investigated. At the outlet BC, due to the highly disturbed flow field, an opening condition with an average static pressure (relative pressure equals to 0 Pa) was fixed.

Walls are defined with no-slip wall BCs.

A second order implicit time stepping was adopted for the time discretization and a time step of 1° with a maximum number of coefficient loops equal to 6 was defined.
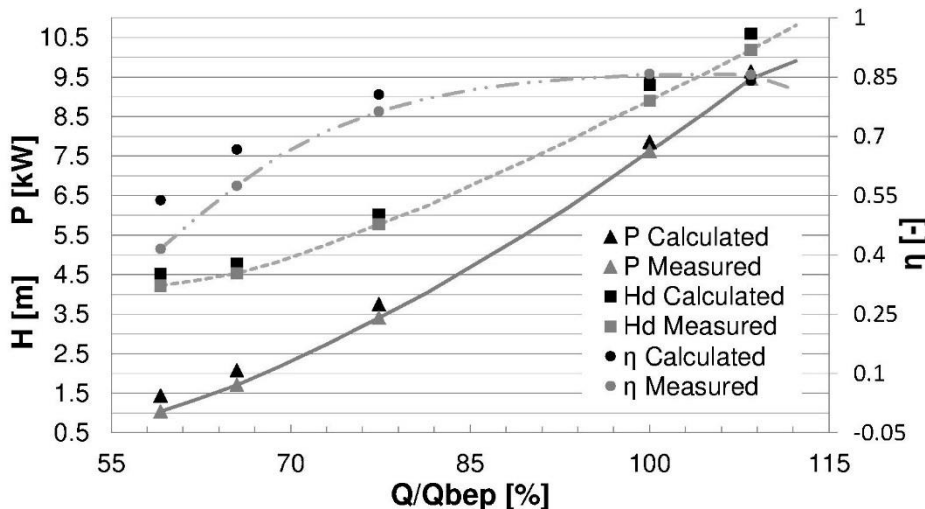
The maximum Courant number resulted to be lower than 3 for all the analyzed flow rates. The resulting RMS values for the residuals were: u momentum $1.6*10^{-5}$, v momentum $1.60*10^{-5}$, w momentum $8.00*10^{-6}$, and turbulence kinetic energy $2.60*10^{-5}$.
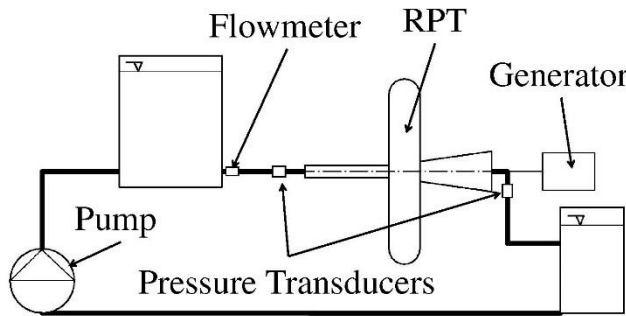
Fig. 4 Scheme of the experimental set-up

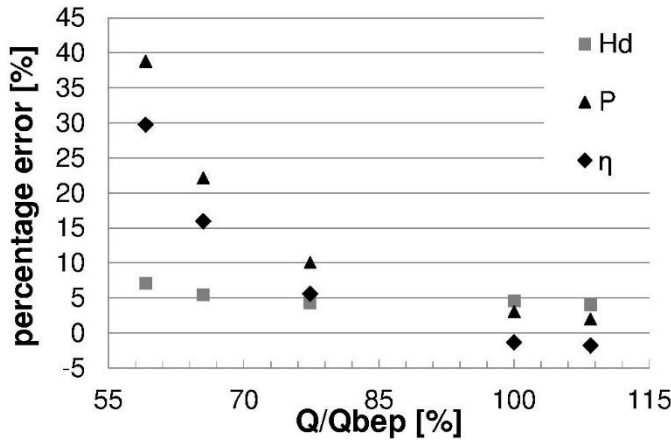## COMPARISON BETWEEN NUMERICAL AND EXPERIMENTAL RESULTS

To validate the numerical model, the numerical performance curves were first compared with those experimentally acquired according to the ISO standards (fig. 4).

Numerical analyses have been carried out for 5 operating points ($59.1\%Q_{bep}$, $65.5\%Q_{bep}$, $77.4\%Q_{bep}$, Q_{bep}, $108.5\%Q_{bep}$) at a rotation rate of 600 rpm and the comparison in terms of head, power and efficiency is reported in fig. 5. The Reynolds number was equal to $5.63*10^6$.

The agreement between numerical and

Fig. 5 Comparison between numerical and experimental performance curves

Fig. 6 Percentage errors between numerical and experimental results

experimental results is quite good in terms of head, with an error smaller than 5% near the best efficiency point and smaller than about 7.5% at partial loads. As regards the mechanical power and the efficiency, the percentage errors between experimental and numerical results significantly increases at partial loads (38% of power error and 29.74% of efficiency error for 59.1%Q_{bep}). However, since the disc friction losses, nearly constant in all the operating conditions, were not considered in the numerical model, an overestimation of both the mechanical power and the efficiency, greater in percentage at partial loads, was expected and seems to justify errors in terms of power and efficiency greater than those obtained in terms of head (fig. 6).

In spite of the simplification related to the friction losses, the numerical model can be considered able to predict with sufficient accuracy the performance of the pump-turbine in the whole operating range.

NUMERICAL SIMULATION OF THE TURBINE BRAKE

In order to catch the onset of the instabilities in the flow field in a load rejection scenario, it is necessary to reproduce the conditions that during turbine brake may lead to the development of rotating stall phenomena and, consequently, to the S-shaped characteristic. From a numerical point of view, it is hence necessary to carry out a simulation with a time-varying boundary condition in which the mass flow rate at the inlet was reduced from 45.1% to 15.9% Q_{bep} in about 20 seconds according to the following equation:

$$Q_m(t)=45.1\%Q_{bep}*\rho\text{-}K*t \qquad [\text{kg } s^{-1}] \qquad (1)$$
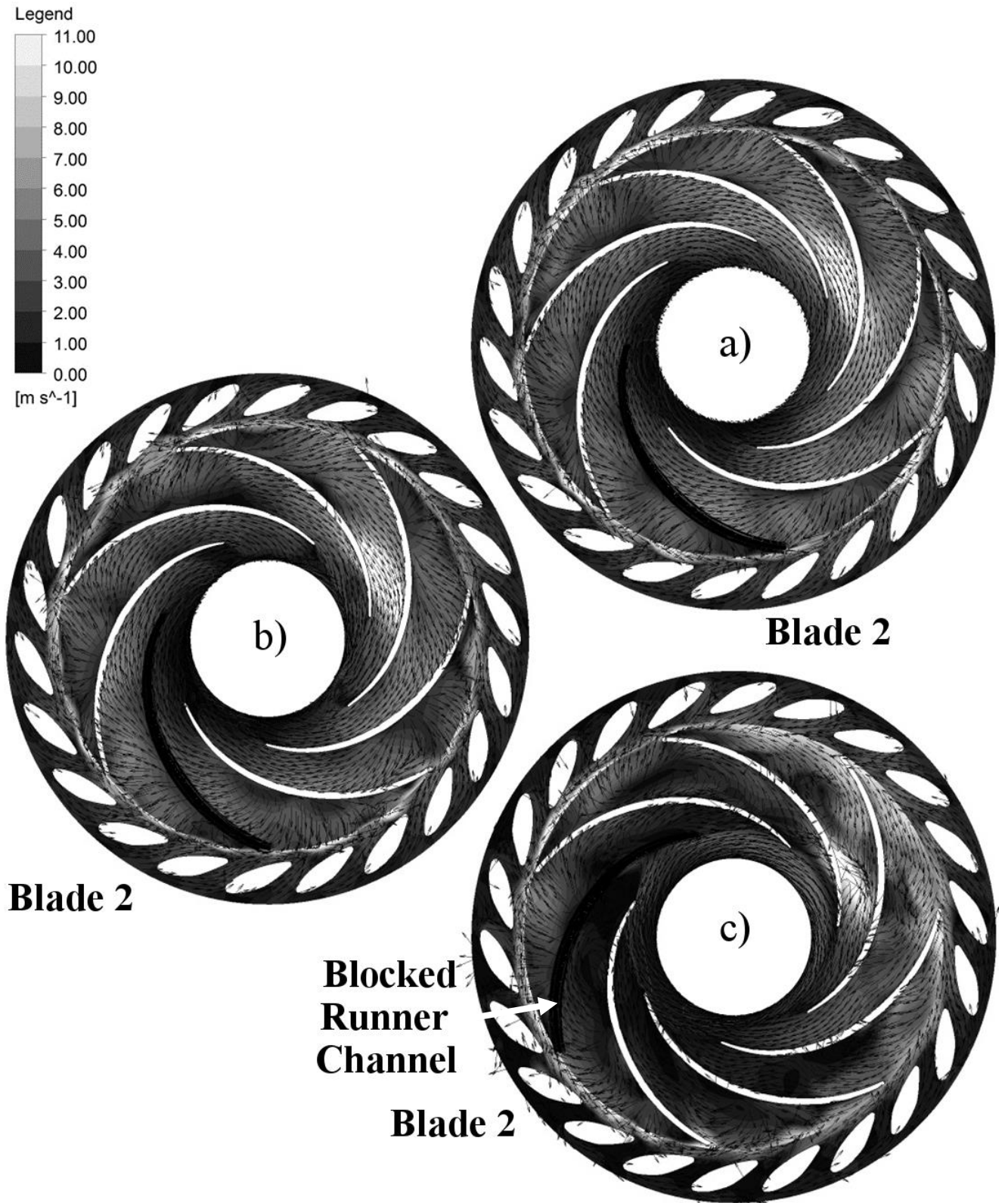
The flow field was initialized with the flow field calculated at Q=45.1%Q_{bep} (P=0.34 kW; η=0.18), slightly above the runaway condition (Q=37.6%Q_{bep}; P=6*10^{-4} kW; η=0.04) where the unstable phenomena was expected to start to develop. The guide vane opening as well as the rotational speed n remained constant during the simulation. 20 complete runner revolutions were simulated to investigate the operating range interested by the development of the rotating stall.

Since the simulation of the turbine brake resulted to be time-consuming, the number of coefficient loops for each time step was reduced to 3, with a time step still equal to 1° of runner rotation. Even thought this modification slightly increase the simulation residuals (u momentum= 1.10*10^{-4}, v momentum=1.10*10^{-4}, w momentum=4.90*10^{-5}, turbulence kinetic energy=1.90*10^{-4}), it resulted not to affect the resulting performance of the pump-turbine on which the validation was based.

RESULTS

Fig. 7 reports the instantaneous velocity fields inside runner and guide vanes for three different instants corresponding to three different flow rates: t_1) 45.1%Q_{bep}, t_2) 37.8%Q_{bep} and t_3) 21.8%Q_{bep}. Fig. 7a represents the velocity field at the beginning of the simulation of the turbine brake (45.1%Q_{bep}). As it can be seen, the onset of flow separations on the blade Pressure Side (PS) starts to slightly perturb the flow field in the first half of the runner channels. During the turbine brake, the progressive reduction of the mass flow rate causes the development and enlargement of these regions of flow separation, with the onset of a back flow near the inlet throat of some channels (fig. 7b). Further reductions of the inlet mass flow rate leads to the full blockage of the flow in some runner channels due to large vortexes developing across the whole passage section (fig. 7c). Since

Fig. 7 Instantaneous velocity flow field inside runner and guide vanes at three different instants: a) $t_1 - Q = 45.1\%Q_{bep}$; b) $t_2 - Q = 37.8\%Q_{bep}$; c) $t_3 - Q = 21.8\%Q_{bep}$

guide vanes are very close to the runner, the flow field development in the distributor is affected by the unsteady phenomena developing in the runner and hence also the wicked vanes channels resulted to be alternately blocked or stalled (fig. 7c).

The blockage action is confirmed by the analysis of the flow rate passing through the channels of
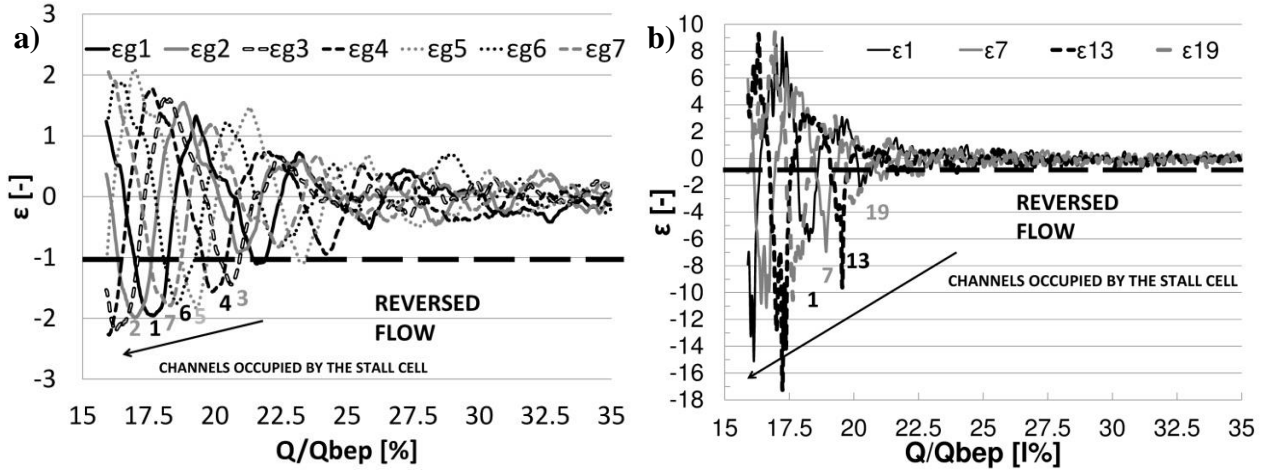
Fig. 8: Evolution of the flow rate passing through each channel of the runner (a) and of the guide vanes (b)
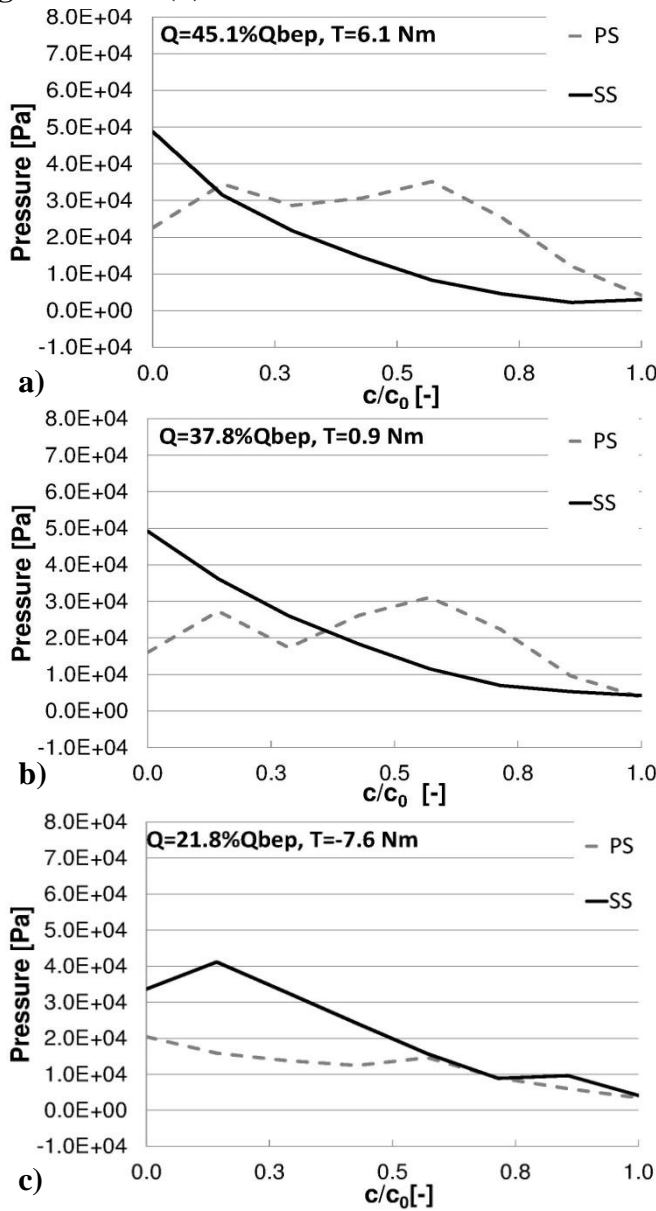
Fig. 9 Pressure distribution along the blade length (blade 2) at mid-span at four different instants: a) Q= 45.1%Q_{bep}; b) Q=37.8%Q_{bep}; c) Q=21.8%Q_{bep}.

runner and guide vanes. Fig. 8 reports the difference in percentage between the instant flow rate q_i, passing through the channel i and the theoretical mean value ($\sum_{i=1}^{n_b} q_{i,}/n_b$):

$$\varepsilon_i = \frac{q_{i,} - \frac{1}{n_b}\sum_{i=1}^{n_b} q_{i,}}{\frac{1}{n_b}\sum_{i=1}^{n_b} q_{i,}} \qquad (i = 1..n_b) \qquad (2)$$

As it can be seen in fig. 8a, during the turbine brake several channels in the runner resulted to be blocked ($\varepsilon_i=-1$; $q_{i,} =0$) or characterized by a back flow ($\varepsilon_i<-1$; $q_{i,} <0$). It is also interesting to notice that the stall cell, partially or fully blocking the regular flow, rotates, according to the runner rotation direction, from one channel to the following one with increasing intensity during the turbine brake.

In the guide vanes the development of the unsteady phenomena seemed to be even more intense with flow rate fluctuations much greater than those characterizing the runner channels (fig. 8b).

During the turbine brake, these unsteady phenomena affected the pressure distribution on the runner blades, modifying their load distribution. Fig. 9 reports the instantaneous pressure distribution on a runner blade (blade 2), located in the perturbed area with increasing intensity of the stall phenomena. The same three instants of fig. 3 have been considered:

$t_1 - Q= 45.1\%Q_{bep}$;
$t_2 - Q=37.8\%Q_{bep}$;
$t_3 - Q=21.8\%Q_{bep}$.
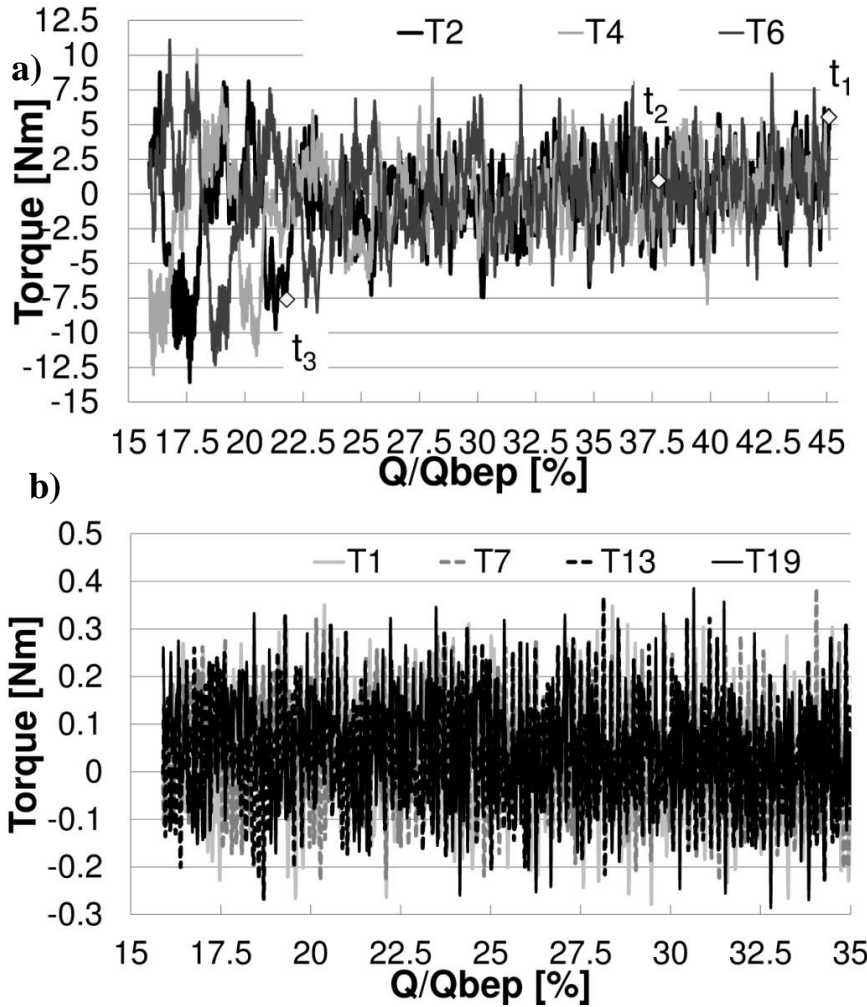
Fig. 10 Evolution of the blade torque during the turbine brake: a) runner (blades 2,4 and 6); b) guide vanes (blades 1, 7, 13 and 19)
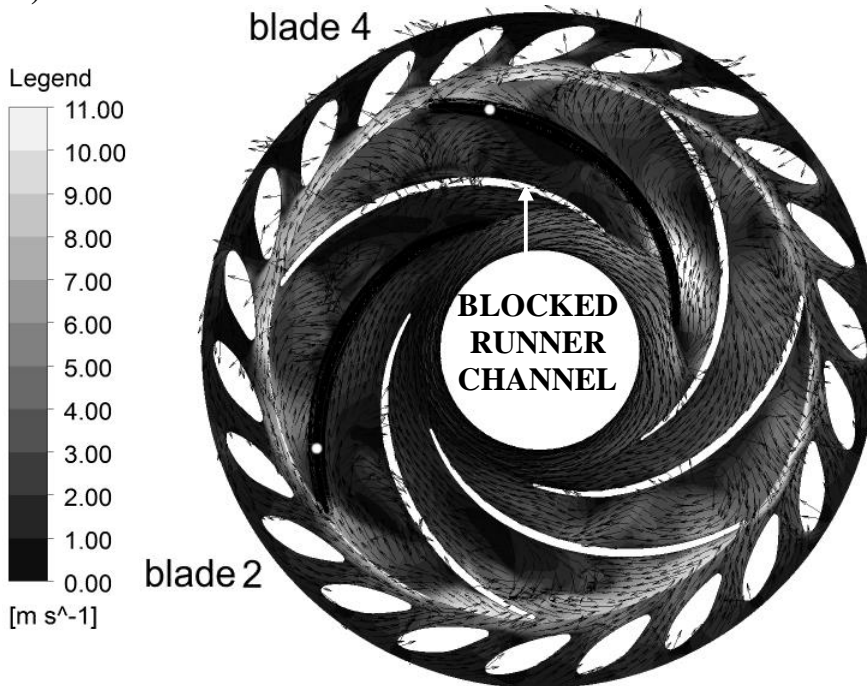
Fig. 11 Instantaneous velocity flow field inside runner and guide vanes for Q= 20.3%Q$_{bep}$

Close to the runaway condition, the flow around blade 2 is perturbed in the very first part of the blade by the onset of flow separations, whereas the remaining part of the blade is properly working (fig. 9a). When the mass flow rate is further reduced and the runner operates below the runaway condition (fig. 9b), quite half of the blade is affected by the unsteady phenomena and the pressure on the suction side (SS) is quite close to that on the pressure side: the blade is stalling (T=0.9 Nm). For smaller mass flow rates (fig. 9c), the channel near blade 2 is completely blocked by a stall cell (fig. 7c) and the pressure on the pressure side (PS) becomes smaller than on the suction side (SS), resulting in a negative torque: the blade behaved as a pump blade (reverse flow).

Due to the rotating characteristics of these stall cells, the blades are characterized by fluctuations in time of the pressure distributions and hence of the torque, depending on the evolution of the flow field around the blade. Figure 10 reports the evolution in time of the torque on three runner blades and four guide vanes during the turbine brake. As it can be seen, the blades are subjected to continuous changes in blade operating mode: from turbine (positive blade torque) to reverse pump (negative blade torque) and vice-versa. For example, blade 2 at the instant t_3 (Q=21.8%Q$_{bep}$) is characterized by a negative torque (T=-6.2 Nm) that becomes positive (T=6.5 Nm)

a few instants later ($Q=20.3\%Q_{bep}$) as a consequence of the displacement of the stall cell in other channels (fig. 11). At this instant the blockage action with increased intensity is mainly interesting blade 4, characterized by an extremely negative torque (T=-10 Nm).

It is interesting to notice that the torque fluctuations on the runner blades increase in amplitude together with the intensity of the unsteady phenomena with negative consequences on the fatigue resistance of the mechanical components.

PERFORMANCE ANALYSIS OF THE PUMP-TURBINE DURING THE TURBINE BRAKE

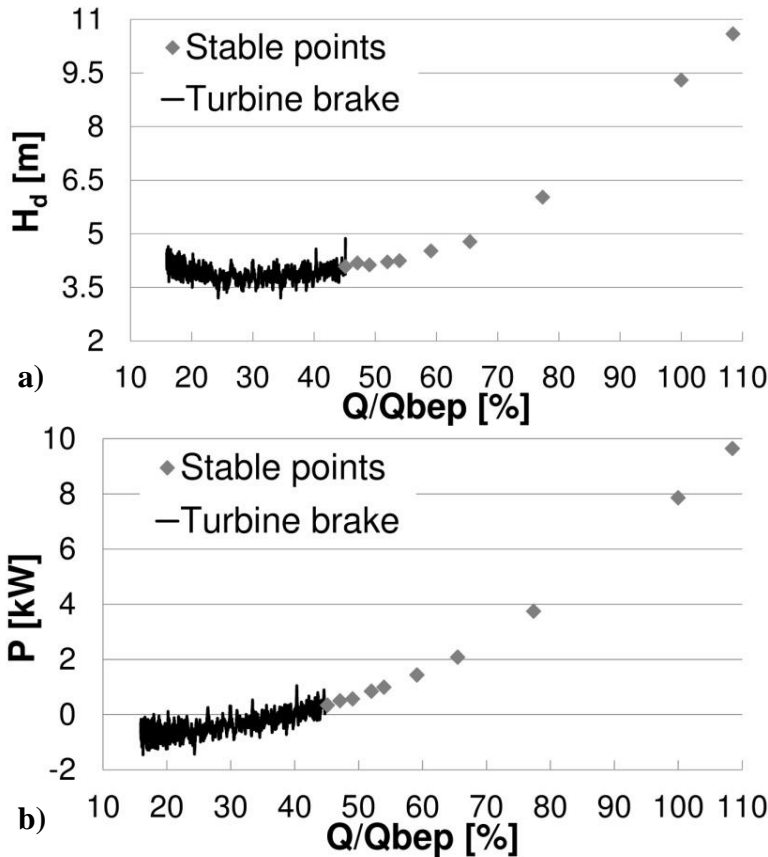Figure 12 reports head and mechanical power of the pump-turbine in the stable operating region (dots representing time- averaged performance values) and their evolution during the turbine brake (continuous black lines). The development of the unsteady phenomena affects the pump-turbine performance, determining an increase in amplitude of the head oscillations. Moreover, when the mass flow reduces from $24.5\%Q_{bep}$, the head of the pump-turbine increases (fig. 12a) and the mechanical power becomes negative (fig. 12b).

In order to better understand the reasons of this change in slope, the total head of the pump-turbine was decomposed on the basis of the contributions of the different components of the pump-turbine:

$$H_d=H_{runner}+H_{GV}+H_{ducts}$$
(3)

Unlike the inlet and outlet ducts whose heads (H_{ducts}) resulted to be nearly constant during the turbine brake, the most important contribution to the increase in H_d resulted to be given by the guide vanes (H_{GV} in fig. 13) suffering from a the more severe blockage action. Even the performance of the runner are negatively affected by the development of the rotating stall, as demonstrated by the significant increase in amplitude of the head oscillations (H_{runner} in fig. 13) determining, for the lowest flow rates, an alternating behaviour:

Fig. 12 Performance curve of the pump-turbine: a) head; b) mechanical power
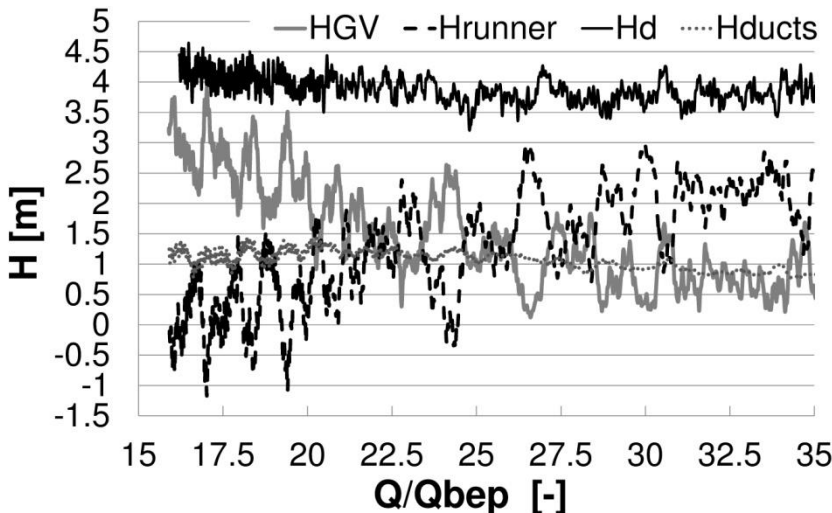
Fig. 13 Contributions in head of the runner and guide vanes

9
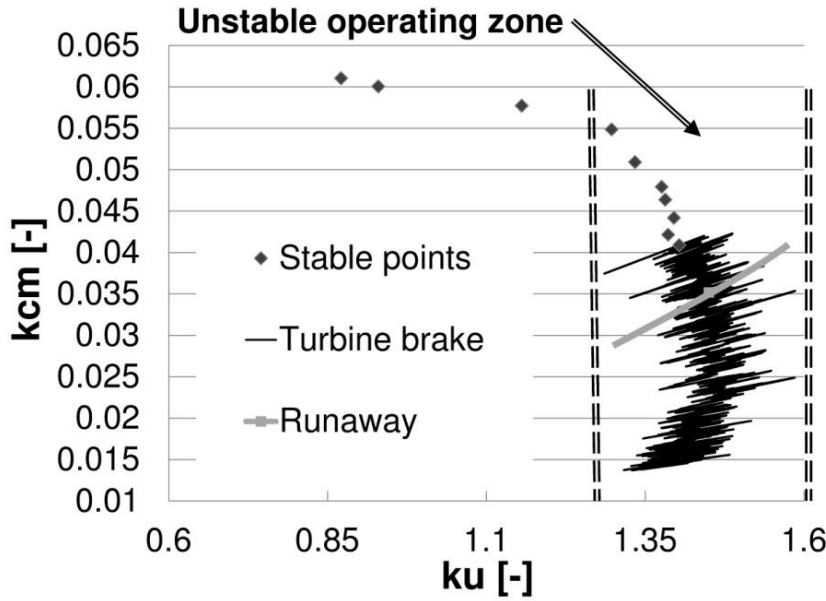
Fig. 14 Numerical dimensionless discharge-speed characteristic curve.

from generating to pumping mode and vice-versa.

The negative slope of the total head curve determines a S-shaped characteristic in dimensionless terms k_{cm} and k_u, defined as follows:

$$k_{cm} = \frac{4\,Q}{\pi D_2^2 \sqrt{2\,g\,H_d}} \quad (4)$$

$$k_u = \frac{U_2}{\sqrt{2\,g\,H_d}} \quad (5)$$

where D_2 is the outer runner diameter, U_2 is the tangential velocity of the runner at the outer diameter, g is the gravity acceleration, Q is the inlet mass flow rate and H_d is the total head.

Figure 14 reports the dimensionless terms (eqs. 4 and 5) calculated in some operating points of the stable area (time-averaged values) and during the turbine brake.

As highlighted above, the unstable behaviour appears and develops with an increase in head for extremely low flow rates ($Q<24.5\%Q_{bep}$), determining a S-shaped discharge-speed curve. However, the existence of this S-Shape in the dimensionless characteristic curve does not only affect the pump-turbine behaviour during load rejection but also further limit the stable operating range of the pump-turbine. In fact, because of this shape, a "theoretically" stable operating point ($Q>24.5\%Q_{bep}$) located in the zone between the double-dashed lines, may jump into an unstable point with the same value of k_u. As a consequence, the real stable (and safe) operating range of the pump-turbine is sensibly reduced and the unstable behaviour cannot be only confined to the above mentioned off-design conditions ($Q<24.5\%Q_{bep}$) but should be significantly extended to greater flow rates ($Q<65.5\%Q_{bep}$). Considering also the even more frequent switching from generating to pumping mode and vice-versa, during which the machine operates in the proximity of the runaway condition, it is obvious the importance of correctly defining the unstable operating area.

CONCLUSIONS

The S-Shaped characteristic in pump-turbines is associated to the development of an unstable behaviour with fluctuations of speed, torque, head and flow rate that negatively affect the startup and synchronization of the pump-turbine with the grid as well as the turbine brake.

This paper presents an in-depth study of the onset and development of the unsteady phenomena causing the unstable behavior of a pump-turbine during the turbine brake.

Transient numerical analyses were carried out on a pump-turbine in stable operating conditions and, to validate the numerical model, including the leakage system, the numerical performance results were compared with the experimental ones, obtaining a satisfactory agreement. Then, starting from a stable operating condition, a numerical analysis, running through the flow speed characteristics up to the pump-turbine brake zone in a load rejection scenario, was carried out. The flow field development was analysed for 20 impeller revolutions with a flow rate decreasing at each time step in order to simulate the real behaviour of the pump-turbine during the turbine brake.

Running through the unstable operating zone, the analysis allowed to identify the onset and the development of stalled cells partially or totally blocking some runner and distributor channels. These cells resulted to move from one channel to the following one according to the rotation direction of

the runner and with increasing intensity. Their onset, enlargement and disappearance was demonstrated to cause fluctuations in time not only of the flow rate passing through the channels both in the runner and in the guide vanes, but also of the pressure distribution and hence of the torque exerted on the blades. These fluctuations increased in amplitude together with the intensity of the unsteady phenomena and, for the low flow rates, became so intense as to cause continuous changes in blade operating mode (from turbine to reverse pump and vice-versa).

As regards the global performance of the pump-turbine, the development of this unstable behaviour resulted to be strictly related with a negative slope of the head curve at part loads ($Q<24.5\%Q_{bep}$), causing the S-Shape in the dimensionless discharge-speed curve at constant guide vane opening. The increase in head resulted to be mainly due to the severe blockage action in the guide vanes channels.

Even if the unsteady phenomena developed for very low flow rates ($Q<24.5\%Q_{bep}$), related to off-design conditions, the existence of the S-Shape in the dimensionless characteristic curve transformed "theoretically stable" operating conditions in possible unstable ones, being equal ku. As a consequence of this S-shape, the stable operating range of the pump-turbine resulted to be significantly reduced from $Q>24.5\%Q_{bep}$ to $Q>65.5\%Q_{bep}$.

REFERENCES

Brennen C. E., (1994), *Hydrodynamics of pumps*, Oxford University Press, Oxford, England.

Gentner C., Sallaberger M., Widmer C., Braun O., (2012), *Analysis of unstable operation of pump turbines and how to avoid it*, HYDRO 2012 Innovative Approaches to Global Challenges, 29-31 October 2012, Bilbao, Spain.

Hasmatuchi V., Farhat M., Roth S., Botero F., Avellan F., (2011a), *Experimental evidence of rotating stall in a pump turbine at off design conditions in generating mode*, J Fluids Eng, vol. 133(5), pp.051104-1/8.

Hasmatuchi V., Farhat M., Roth S., Botero F., Avellan F., (2011b), *Hydrodynamics of a pump turbine at off design conditions in generating mode: experimental investigation*, SHF Conference on Cavitation and Hydraulic Machines, 26-27 May 2011, Lausanne, Switzerland.

Olimstad G., Nielsen T., Børresen B., (2012a), Dependency on runner geometry for reversible pump turbine characteristic in turbine mode of operation, J Fluids Eng, vol. 134, pp. 121102-1/9.

Olimstad G., Nielsen T., Børresen B., (2012b), Stability limits of reversible pump turbines in turbine mode of operation and measurements of unstable characteristic, J Fluids Eng, vol. 134, pp. 111202-01/08.

Pejovic S., Zhang Q., F., Karney B., Gajic A., (2011), *Analysis of pump-turbine S instability and reverse waterhammer incidents in hydropower systems*, 4th Int Meeting on Cavitation and Dynamic problems in Hydraulic Machinery Systems, October 2011, Belgrade, Serbia.

Seidel U., Koutnik J., Martin G., *S-curve characteristic of pump-turbines*, HYDRO 2012 Innovative Approaches to Global Challenges, 29-31 October 2012, Bilbao, Spain.

Sun H., Xiao R., Liu W., Wang F., (2013), Analysis of the S characteristic and pressure pulsation in a pump turbine with misaligned guide vanes, J Fluids Eng, vol. 135(5), pp. 051101-1/6.

Wang L Q, Yin J L, Jiao L et al., (2011), *Numerical investigation on the "S" characteristic of a reduced pump turbine model*, Sci China Ser E, vol. 54(5), pp. 1259-1266.

Zhou J. X., Karney B. W., Xu J. C., (2011), *Analytical study on possible self-excited oscillation in S-shaped regions of pump turbines*, P I Mech Eng A – J POW, vol. 225(8), pp. 1132-1142.